Generalized optimal stopping for decision making in energy markets

Frank Heinz[a] and Reinhard Madlener[b,c,*]

[a]RWTH Aachen University, Templergraben 55, 52056 Aachen, Germany
[b]Chair of Energy Economics and Management, Institute for Future Energy Consumer Needs and Behavior, School of Business and Economics / E.ON Energy Research Center, RWTH Aachen University, Mathieustrasse 10, 52074 Aachen, Germany
[c]Department of Industrial Economics and Technology Management, Norwegian University of Science and Technology (NTNU), Sentralbygg 1, Gløshaugen, 7491 Trondheim, Norway

February 2023, updated October 2023

Abstract

This article presents a generalized method for multi-dimensional optimal stopping, tailored to problems that arise in electricity markets, when addressing decisions under uncertainty with Real Options Analysis. Electricity markets are highly transparent with supply and demand volumes available as high-resolution time series and with a fair transparency on production costs. Both supply and demand show strong periodic behavior in the form of, e.g., standard load profiles or similar, making mean-reverting stochastic processes with periodic time-dependent trend functions a good choice for modeling the dynamics. However, this class of problems does not fit well to established methods for optimal stopping – e.g., reducing dimensions or making use of properties of the reward function – and therefore, we propose an alternative, generalized approach. We derive a general form of the Hamilton-Jacobi-Bellman equation instead and propose a numerical solution via the Bellman-Howard operator iteration. We demonstrate the functionality of this approach by setting up an example which represents the retrofit of an electrolyzer to an offshore wind farm. We solve the optimal stopping problem numerically and show that the method supports decision making well on such an irreversible investment under uncertainty.

Keywords: Real Options, Stochastic Mean-Reverting Processes with Time-Dependent Trend, Optimal Stopping, Decision Making under Uncertainty
JEL Classification Nos.: C61, D81, G11

1 Introduction

Real Options Analysis is well established for decision making concerning irreversible investments under uncertainty. Either via tree-based models (cf. [15]), contingent claims analysis or dynamic programming, various option values like the value to wait can be determined and thus optimal decisions found. Among the solution methods available, dynamic programming is the most generic

*Corresponding author. Tel: +49-241-80 49 820.
E-mail: RMadlener@eonerc.rwth-aachen.de (R. Madlener).

one; however, it comes with considerable mathematical complexity. The main approach in dynamic programming therefore is to first reduce any problem to only one dimension without explicit time dependency, for which solution methods exist (e.g., [8] for general Itô processes), or to leverage that an underlying stochastic process is one-dimensional, before mathematical solutions are determined. Multidimensional stopping problems have been researched as well, with results for, e.g., reward functions given as positive definite quadratic forms (Ref. [6]) or for monotone reward functions, using a Doob-Meyer decomposition approach (Ref. [7]).

However, when researching the energy sector and electricity markets in particular, in many cases it is difficult to reduce the dimensions or to postulate certain properties of the reward function. At the same time, one outstanding characteristics is that supply and demand volumes are very transparent – high-resolution time series are typically available – and are dominated by periodic behavior. Such dynamics can be modeled well with mean-reverting processes with explicit time dependency, so-called one-factor Hull-White models (Ref. [20]), or, to avoid negative values for electricity demand and supply, with Inverse-Gamma dynamics (Refs. [27] and [28]). Further, also production costs are fairly transparent. This allows to model the pricing dynamics with a rather simple diffusion process[1] which is using supply and demand (cf. [2]) compared to mathematically more complex jump-diffusion models as these advocated in, e.g., [3] or [18].

Making use of these specific properties, we suggest an alternative approach to multi-dimensional optimal stopping. We derive a general Hamilton-Jacobi-Bellman equation that is applicable to a system of mean-reverting stochastic differential equations with periodic trend functions. This system captures the pricing dynamics well, it allows to add intermittent power sources and it enables us to model potential stochastic dependencies among the underlying Brownian motions. It allows long-term price forecasts by making use of the existing long-term forecasts of supply and demand which are available from research related to the ongoing energy transition (see, e.g., the meta study [37], or the detailed study [32]). By doing so, it allows to research optimal stopping in the energy market under realistic assumptions. Further it contributes to quantifying the so-called merit order effect in the energy market, i.e., the expected electricity price reduction in the day-ahead market, due to a rise in renewable power generation (see [38] for a literature overview). Hence, this setup expands the theory of Real Options to a relevant class of research problems in today's electricity markets.

We complete this approach by adding the solution method of a Bellman-Howard operator iteration and finally suggest an implementation architecture. We demonstrate its usefulness by setting up the example of an investment decision with relevance for energy policy making – the retrofit of a subsidy-free offshore wind farm with an electrolyzer, i.e., one particular type of equipment that is needed in addition to renewable power generation equipment for a successful energy transition – and show that for this kind of dynamics, the option value to wait (i.e., to defer the investment) can be determined by setting up and solving the corresponding optimal stopping problem numerically.

This article is structured as follows. In section 2, we derive the generalized stopping problem. In section 3, we introduce the illustrative example. Some sources and basic calculation results for

[1] In the mathematical literature, the term diffusion process is frequently used for stochastic processes driven by a Brownian motion, since in applications outside economics, these processes can be used to describe, e.g., the diffusion of heat in a material or similar phenomena. Correspondingly, jump-diffusion processes denote a combination of a Poisson process with a Brownian motion.

this section we have moved to the appendix. In section 4, we determine numerical solutions before we discuss the results in section 5, draw conclusions on the practical applicability and finally close with an outlook for further research.

2 The generalized Methodology

In this section, we introduce the dynamics of stochastic, positive mean-reverting processes with periodic, time-dependent trend functions for supply and demand, for the production volume of a hypothetical asset and introduce the merit order curve for the electricity price. Based on this setup of price and volume over time, we derive the Hamilton-Jacobi-Bellman equation, restricted to the subset of discounted value functions and end this section with proposing a software architecture for implementation, e.g., in `C++`.

2.1 The underlying dynamics

We formulate our electricity price model in the style of [2] and expand it in several ways. Already [2] suggests time-dependent trend functions: let $X_t = (X_t^{(1)}, X_t^{(2)})$ be a two-dimensional stochastic process with $X_t^{(1)}$ representing the renewable supply and $X_t^{(2)}$ representing the demand. Then, the one-factor Hull-White model of the form

$$dX_t = \Theta(\mu(t) - X_t)dt + \sigma dW_t\,, \tag{1}$$

with trend functions restricted to linear combinations of sin and cos including intercept, captures the dynamics well. Here, dW_t is the increment of a two-dimensional Brownian motion and $\sigma, \Theta \in \mathbb{R}^{2\times 2}$ are constant, diagonal matrices, whose components can be identified with empirical data. There exists an analytical solution to eq. (1) and it can easily be shown that under the restriction imposed on the trend functions, the expected value approximates $\mu(t)$ for $t \to \infty$, which is the desired behavior of the dynamics. However, the paths of the solutions to this model can have negative values. A further expansion to an Inverse Gamma model

$$dX_t = \Theta(\mu(t) - X_t)dt + \tilde{\sigma}(t)X_t dW_t \tag{2}$$

avoids this while at the same time, it preserves the desired dynamical properties. Ref [28] shows, by approximating eq. (2) with a discrete ARCH scheme, that the paths remain positive as long as $\mu(t)$ and Θ are positive (ibid, section 2). Ref. [27] shows that for a constant μ, the expectation shows the desired property $E \to \mu$ (ibid, p.22). Further, from both references it can be derived that Θ and μ stay the same as for the Hull-White dynamics, while in each dimension, the volatility coefficient σ is

$$\sigma_i(t) = 2\,\Theta_{i,i}\sqrt{\frac{\sigma^2_{X^{(i)}}}{\mu^{(i)}(t)^2 + 2\Theta_{i,i}\,\sigma^2_{X^{(i)}}}}\,, \quad \mathrm{i} = 1,\, 2. \tag{3}$$

The coefficients of eq. (2) are globally Lipschitz and growth limited[2], so finally with [22], p.289, we can conclude that $E||X_t||^2 < \infty$ and from that, we derive that also for a time-dependent trend,

[2]This property is required later for optimal stopping, too – thus, another well-known positive short-rate model, the ECIR model, cannot be used because it is not globally Lipschitz.

we have $E \to \mu(t)$, as long as $\mu(t)$ is restricted as stated above.

Having an inelastic demand, the electricity price is determined by a supply function F that on the one hand incorporates random renewable power generation into the merit order curve representing the supply side and on the other hand takes the random demand as an input. When studying a current merit order curve in e.g., the bidding zone DE_LU[3] of the day-ahead market for electricity in Germany and Luxembourg, as given, e.g., in [19], we show that the function

$$F(x_1, x_2) = c_2 \arctan\left(\frac{x_2}{c_1 + c_4 x_1}\right) + c_3 \left(1 + \alpha \frac{x_2 - x_1}{c_1}\right)^{1/\alpha} \tag{4}$$

can be used. The variable x_1 represents the random part of the power supply, the variable x_2 represents the random demand for power. A full pricing model for the electricity price S_t^E is

$$\begin{aligned} dX_t &= \Theta(\mu(t) - X_t)dt + \sigma(t, X_t)dW_t \\ S_t^E &= F_{\alpha, c_i}(X_t)\,. \end{aligned} \tag{5}$$

Because of the fundamental-stochastic approach of this model (taxonomy cf. [36]), the future energy system can be estimated, a step which is impossible if relying on statistics of current empirical data alone. Another advantage is that it is mathematically much less complex than other models such as these advocated in, e.g., [3] or [18]. The parameters c_i are used to calibrate the supply function to a current merit order curve. Making the parameters c_i time-dependent, the model finally can handle an extrapolation from today to an expected future merit order curve.

The dynamics for the price can be found by expanding F and using the differential equation for X_t:

$$\begin{aligned} dS_t^E &= \frac{\partial F}{\partial t}(t, X_t)\, dt + \nabla F(t, X_t)\, dX_t + \frac{1}{2}\, \Sigma_{i,j=1}^2 \frac{\partial^2 F}{\partial x_i \partial x_j}(t, X_t)\, d[X^{(i)}, X^{(j)}]_t \\ &= \left(\frac{\partial F}{\partial t} + \frac{1}{2}\left(\frac{\partial^2 F}{\partial x_1^2}\sigma^2_{X^{(1)}} X_t^{(1)} + \frac{\partial^2 F}{\partial x_2^2}\sigma^2_{X^{(2)}} X_t^{(2)}\right) + \nabla F\, \Theta\, (\mu(t) - X_t)\right) dt + \nabla F \sigma\, dW_t \\ &= S_1(t, X_t)\, dt + S_2(t, X_t)\, dW_t \quad \text{a.s.} \end{aligned}$$

with differentiable functions $S_1 : \mathbb{R}^2 \times [0, \infty) \to \mathbb{R}$ and $S_2 : \mathbb{R}^2 \times [0, \infty) \to \mathbb{R}^2$ for abbreviation. This expansion shows that the volatility of the electricity price is $\|\nabla F \sigma\|$, i.e., it is driven by the slope of the merit order curve, the volatility of renewable electricity supply and electricity demand, and its trend functions[4].

We complete the underlying dynamics by adding the electricity production volume of an asset to be analyzed in the form of another Inverse Gamma mean-reverting stochastic process of the form

$$dQ_t = \zeta\, (\kappa(t) - Q_t)\; dt + \sigma_Q(t, Q_t)\, dW_t\,, \tag{6}$$

which in practical problems can be used either for modeling the climatic drivers of renewable power production (wind speed, solar radiation) or for the power itself. In our example later on, we

[3] A bidding zone is the largest geographical area within which market participants are able to exchange energy without capacity allocation [29]. The bidding zone DE_LU (EIC Code 10Y1001A1001A82H) has been introduced at the beginning of 2019 and includes the two countries Germany and Luxembourg [12].

[4] Note that $\nabla F \sigma dW_t = \|\nabla F \sigma\|\, d\tilde{W}_t$ for a one-dimensional Brownian motion $d\tilde{W}_t$.

derive the power rate Y_t from wind speed data with a so-called power curve P, which is a property of the wind turbines used, i.e., $Y_t = P(Q_t)$:

$$\begin{aligned} dY_t(Q_t) &= \frac{\partial P}{\partial x}(Q_t)\, dQ_t + \frac{1}{2}\frac{\partial^2 P}{\partial x^2}(Q_t)\, \sigma_Q^2 dt \\ &= \left(\frac{\partial P}{\partial x}(Q_t)\zeta\left(\kappa(t) - Q_t\right) + \frac{\sigma_Q^2}{2}\frac{\partial^2 P}{\partial x^2}(Q_t) \right) dt + \sigma_Q \frac{\partial P}{\partial x}(Q_t)\, dW_t \\ &= Y_1(t, Q_t)\, dt + Y_2(t, Q_t)\, dW_t \quad \text{a.s.} \end{aligned}$$

with differentiable functions $Y_1, Y_2 : \mathbb{R} \times [0, \infty) \to \mathbb{R}$.

The explicit time dependency needs to be normalized, i.e., treated as a third space dimension. For this, we define the stochastic process $Z_t = t$ with its obvious differential equation $dZ_t = dt$. The complete system finally reads

$$d\Gamma_t = B(\Gamma_t)dt + \Lambda(\Gamma_t)dW_t\,,$$

with $\Gamma_t = (S_t^E, Y_t, Z_t)$, $B \in \mathbb{R}^3$, $\Lambda \in \mathbb{R}^{3\times 2}$ and W_t being a two-dimensional Brownian motion. Note that the two dimensions of W_t are not necessarily stochastically independent from each other. In real-world problems, we may encounter a cross-correlation between the electricity price and the electricity production, see, e.g., the recent research in Ref. [23] or see our example in subsection 3.3. This can be implemented in the model by using suitably correlated series of random numbers in the numerical solution (see, e.g., [27], p.4).

2.2 The optimal stopping problem

Next, we formulate the optimal stopping problem adapted to this dynamics. For this, we follow the rather general theory presented in [26] on a heuristical level, with occasional cross-references to [9]. Proofs of the respective statements can be found in [26].

Let $v^{(u)}(x,t)$ be a momentary value at a time t and at a point $x \in \mathbb{R}^2$, controlled by a control process u_t. Then, for one chosen strategy u_t, the value of one individual complete trajectory along Γ_t, over the complete time horizon, is

$$\nu^{(u)}(\Gamma_0) = \int_0^\infty v^{(u_t)}(\Gamma_t)\, dt\,,$$

and the project value is the mean of the momentary value function along all trajectories Γ_t:

$$V^{(u)}(\Gamma_0) = E\left[\nu^{(u)}(\Gamma_0)\right] = E\left[\int_0^\infty v^{(u_s)}(\Gamma_s)ds\right].$$

The general optimization problem is to find an optimal control strategy u_t such that the project value $V^{(u)}(\Gamma_0)$ is maximized[5]:

$$V(\Gamma_0) = \sup_u \left\{ V^{(u)}(\Gamma_0) \right\} = \sup_u \left\{ E\left[\int_0^\infty v^{(u_s)}(\Gamma_s)ds\right] \right\}. \tag{7}$$

[5]Please note that while every project value starts at 0 at the beginning for every starting point Γ_0, the trajectories of Γ_t depend on its starting point and, therefore, $V^{(u)}$ and V depend on the starting point, too.

We restrict the control process u_t to stopping, i.e., to a problem of the form

$$V(\Gamma_0) = \sup_{t^*} \left\{ E\left[\int_0^{t^*} v_1(\Gamma_s) ds + v_2(\Gamma_{t^*}) \right] \right\}, \tag{8}$$

in which the problem requires to find the stopping time t^*. The momentary value v_1 provides a potential pay-off before t^*, the function v_2 provides the value after stopping. Further, following [9], we require any payoff function to be of the form $g^{(u_t)}(t, \Gamma_t)e^{-\rho t}$ with a bounded function g and a discounting factor with discount rate ρ. Following [26], the value function is of the same form, i.e. $\exp(-\rho t)V(\Gamma_t)$, and thus

$$\left.\frac{\partial(e^{-\rho t}V)}{\partial t}\right|_{t=0} = -\rho V(\Gamma_0) + e^{-\rho t}\left.\frac{\partial V}{\partial t}\right|_{t=0} = -\rho V(\Gamma_0) + \frac{\partial V}{\partial t}(\Gamma_0) \tag{9}$$

as well as

$$\left.\frac{\partial(e^{-\rho t}V)}{\partial x}\right|_{t=0} = \frac{\partial V}{\partial x}(\Gamma_0) \quad \text{and} \quad \left.\frac{\partial(e^{-\rho t}V)}{\partial y}\right|_{t=0} = \frac{\partial V}{\partial y}(\Gamma_0)\,. \tag{10}$$

Going back to eq. (8), this deterministic stopping can be approximated by randomized stopping, which finally leads to Bellman's differential equation. We use the control process u_t as an intensity rate that switches between v_1 and v_2. At first, we set

$$U(t) = \exp\left(-\int_0^t u_s\, ds \right).$$

We define u_t such that U is the probability that Γ_t does not stop until time t. Then, $u_t \Delta t + o(\Delta t)$ is the probability that stopping occurs in $[t, t+\Delta t]$ and, finally, $u_t\, U(t)\, \Delta t + o(\Delta t)$ is the probability that stopping does in fact occur in the interval $[t, t+\Delta t]$ and not earlier.

The value of an individual trajectory that is controlled in this way is the sum of its value gained up to any time t if stopped at that time, probability-weighted over all t, plus the value gained if not stopped at all (which can have a probability > 0), weighted with its respective probability:

$$\nu^{(u)}(\Gamma_0) = \int_0^\infty \nu_t(\Gamma_0) u_t U(t)\, dt + \int_0^\infty v_1(\Gamma_t)\, dt\, \exp\left(-\int_0^\infty u_s ds \right)$$

(see Ref. [26], p.10). We note that $dU/dt = -u_t U(t)$ and use the abbreviation $W(t) = \int_0^t v_1(\Gamma_s) e^{-\rho s} ds$ for the integral term in ν_t. Replacing ν_t gives

$$\begin{aligned}
\nu^{(u)}(\Gamma_0) &= \int_0^\infty \left(W(t) + v_2(\Gamma_t)\right) u_t U(t)\, dt + \int_0^\infty W'(t)\, dt \exp\left(\int_0^\infty u_s ds \right) \\
&= \int_0^\infty v_2(\Gamma_t) u_t U(t)\, dt - \int_0^\infty W(t) U'(t)\, dt + \int_0^\infty W'(t)\, dt \lim_{t\to\infty} U(t)\,.
\end{aligned}$$

Using the fact that $W(0) = 0$, we have $\int_0^\infty W'(t) dt = \lim_{t\to\infty} W(t)$. Assuming that all limits exist we can formulate

$$\nu^{(u)}(\Gamma_0) = \int_0^\infty v_2(\Gamma_t) u_t U(t) dt - \int_0^\infty W(t) U'(t) dt + \lim_{t\to\infty} \left(W(t) U(t)\right)\,.$$

We observe that $U(0) = 1$ and hence, we can further write $W(t)U(t) = \int_0^t (W(s)U(s))' \, ds$ and then integrate by parts:

$$\begin{aligned}\nu^{(u)}(X_0) &= \int_0^\infty v_2(\Gamma_t) u_t U(t) dt - \int_0^\infty W(t) U'(t) dt + \int_0^\infty (W(t)U(t))' \, dt \\ &= \int_0^\infty v_2(\Gamma_t) u_t U(t) dt + \int_0^\infty W'(t) U(t) dt \\ &= \int_0^\infty v_2(\Gamma_t) u_t U(t) + v_1(\Gamma_t) U(t) dt \, .\end{aligned}$$

This, combined with eq. (7), leads to the project value in the case of randomized stopping:

$$V(\Gamma_0) = \sup_u \left\{ E\left[\int_0^\infty v_1(\Gamma_s) U(s) + v_2(\Gamma_s) u_s U(s) ds \right] \right\} . \tag{11}$$

In this sense, eq. (8) turns into the limit over a sequence of more and more sharpened intensities u in eq. (11). We restrict the problem further. For establishing the option value to wait, during waiting there is no pay-off but only a potential capital gain, thus $v_1 \equiv 0$. Applying Bellman's principle, we see that

$$V(\Gamma_0) = \sup_u \left\{ E\left[\int_0^t v_2(\Gamma_s) u_s U(s) ds \right] + E\left[V(\Gamma_t) \right] \right\} .$$

Expanding $V(\Gamma_t)$ by Itô's lemma (in integral form) yields[6]:

$$0 = \sup_u \left\{ E\left[\int_0^t v_2(\Gamma_s) u_s U(s) ds \right] + E\left[\int_0^t \nabla V B - \rho V + \frac{1}{2} \left(\Lambda_{11}^2 \frac{\partial^2 V}{\partial x^2} + \Lambda_{22}^2 \frac{\partial^2 V}{\partial y^2} \right) ds \right] \right\} . \tag{12}$$

Here, we used that $V = 0$ at $t = 0$, and we used equations (9) and (10). The control process u_t is unbounded, therefore, in eq. (12), in order to come to a suitable differential equation, a further coordinate transformation is required. Let $m = (1 + u_t)^{-1}$ and observe that for an otherwise unbounded intensity rate u_t, the functions m and $m \cdot u$ are positive and bounded. With our restrictions imposed on the trend functions, with the merit order curve F and (if used) the power curve P, we ensure that the coefficients of the differential equations are bounded as well and so are $\sqrt{m\Lambda_{ij}}$ and mB. Note further that

$$\Psi_t = \int_0^t (1 + u_s) \, ds < \infty \quad \text{for all } t < \infty \text{ and } \Psi_\infty = \infty \, .$$

The new randomized time $\tau_t = \Psi^{-1}$ is defined on $[0, \infty)$ and $\tau_\infty = \infty$. Replacing $t = \tau_s$ and $H_s = \Gamma_{\tau_s}$ yields

$$\begin{aligned}\int_0^\infty U(t)(v_2(\Gamma_t)u_t) dt &= \int_0^\infty \exp\left(- \int_0^t u_s ds \right) (v_2(\Gamma_t) u_t) \, dt \\ &= \int_0^\infty \exp\left(- \int_0^s \frac{u_y}{1 + u_y} dy \right) \left(\frac{u_s}{1 + u_s} v_2(H_s) \right) ds \, ,\end{aligned}$$

[6] We denote $\nabla = (\partial_x, \partial_y, \partial_z)$, i.e., we have the time derivative included as the third space dimension.

with a process H_s that solves

$$H_s = \Gamma_0 + \int_0^s \frac{B(H_y)}{1+u_y}\,dy + \int_0^s \left(\sqrt{\frac{\Lambda_{ij}}{1+u_y}}\right)_{ij} d\xi_y\,.$$

Here, ξ is a two-dimensional Wiener process which equals

$$\xi_\tau = \int_0^{\tau_s} \sqrt{1+u_s}\,dW_s\,.$$

With this time shift it can be shown that

$$0 = \sup_{u_0\geq 0} \frac{1}{1+u_0}\left\{v_2(\Gamma_0)u_0 - u_0 V + \nabla V B - \rho V + \frac{1}{2}\left(\Lambda_{11}^2\frac{\partial^2 V}{\partial x^2} + \Lambda_{22}^2\frac{\partial^2 V}{\partial y^2}\right)\right\}.$$

Furthermore, with $\varepsilon = \frac{1}{1+u_t}$ we can model the behavior of the intensity rate u in the interval $[0,1]$ and write

$$0 = \sup_{\varepsilon\in[0,1]} \left\{\varepsilon\left(\nabla V B - \rho V + \frac{1}{2}\left(\Lambda_{11}^2\frac{\partial^2 V}{\partial x^2} + \Lambda_{22}^2\frac{\partial^2 V}{\partial y^2}\right)\right) + (1-\varepsilon)(v_2 - V)\right\}.$$

This equation is linear in ε. For the interior $\varepsilon \in (0,1)$, there exists only the trivial solution $V \equiv v_2 \equiv 0$ which can be disregarded. On the edges, $\varepsilon = 0$ is an interesting special case. Here we have $v_2 = V$, which means that the value can come only from the investment if there is any value at all, implying either to immediately invest or never invest, i.e., this is equivalent to the classical criterion $NPV > 0$. On the other end, at $\varepsilon = 1$, it is obvious that we cannot have $V < v_2$. Otherwise, because of continuity, for a small shift $1-\varepsilon$, we would contradict the supremum. Instead, we find two conditions (cf. [26]):

$$0 \geq \nabla V B - \rho V + \frac{1}{2}\left(\Lambda_{11}^2\frac{\partial^2 V}{\partial x^2} + \Lambda_{22}^2\frac{\partial^2 V}{\partial y^2}\right) \quad \text{for } V \geq v_2 \tag{13}$$

$$0 = \nabla V B - \rho V + \frac{1}{2}\left(\Lambda_{11}^2\frac{\partial^2 V}{\partial x^2} + \Lambda_{22}^2\frac{\partial^2 V}{\partial y^2}\right) \quad \text{for } V > v_2\,. \tag{14}$$

Eqs. (13) and (14) finally can be combined into

$$v_2 - V + \left[\nabla V B + (1-\rho)V + \frac{1}{2}\left(\Lambda_{11}^2\frac{\partial^2 V}{\partial x^2} + \Lambda_{22}^2\frac{\partial^2 V}{\partial y^2}\right) - v_2\right]_+ = 0\,, \tag{15}$$

which, in its general form as given in [26] p.13, is called Bellman's equation for optimal stopping of a controlled process. Here, eq. (15) is already adapted to our problem with its dimensions, with the specific components of the underlying differential equations, their normalized time dependency and with restricting V to a family of functions with discounting. The brackets $[\cdot]_+$ denote the positive part of the interior and are calculated as $[x]_+ = 1/2(|x| - x)$.

2.3 Numerical solutions and implementation

As numerical solution method, we propose the Bellman-Howard method which iterates the operator derived from the functional equation (15). Here, we assume that $v_2 > 0$ in some subset

(otherwise, the investment can be dropped). Then, let us define the operator

$$\Phi(V) \coloneqq v_2(\Gamma_0) + \Bigg[B_1(\Gamma_0)\frac{\partial V}{\partial x}(\Gamma_0) + B_2(\Gamma_0)\frac{\partial V}{\partial y}(\Gamma_0) + \frac{\partial V}{\partial t}(\Gamma_0) + (1-\rho)V(\Gamma_0) + \frac{1}{2}\left(\Lambda_{11}^2(\Gamma_0)\frac{\partial^2 V}{\partial x^2}(\Gamma_0) + \Lambda_{22}^2(\Gamma_0)\frac{\partial^2 V}{\partial y^2}(\Gamma_0) \right) - v_2(\Gamma_0) \Bigg]_+ \quad \text{for all } \Gamma_0,$$

the stopping time t^* as being the smallest time such that

$$V(S_t^E, Y_t, t) \geq v_2(S_t^E, Y_t, t) \quad \text{for} \quad 0 \leq t \leq t^*$$

($t^* = 0$ or $t^* = \infty$ possible), and the continuation region

$$\mathcal{C} = \{\Gamma \in \mathbb{R}^2 \times [t^*, \infty) \,|\, V(\Gamma) \geq v_2(\Gamma)\}\,.$$

Next, we define the set A as the closure of

$$\mathbb{R}^2 \times [0, \infty) \cap \{Y > 0\}\,.$$

A allows negative prices but requires that the electricity production can be arbitrarily small but necessarily positive, which is a sufficient approximation of the real operations of any power generation asset to be analyzed. This set can be restricted further based on economic criteria, i.e., upper limits on price, production and time. Furthermore, in our model, any such set fulfills the necessary and sufficient criterion defined in [26], pp.203ff. This criterion requires that for all $x \in A$, a number $\delta > 0$ shall exist such that $(\Lambda\Lambda^{\mathrm{tr}}x)x \geq \delta$. This holds true because $\Lambda\Lambda^{\mathrm{tr}}$ is positive semi-definite and positive definite when projected into the subspace $\mathbb{R}^2$. Then the value of waiting V is given by

$$\lim_{n\to\infty} \Phi^n(V(\Gamma)) = V(\Gamma) \quad \text{for} \quad \Gamma \in A \cap \mathcal{C}\,,$$

which can be approximated by iterating the operator Φ.

The set $\mathcal{C} \cap A$ can be empty, which means that immediate investment ($v_2 \geq 0$) or dropping the project ($v_2 < 0$) is preferable over waiting. In the set $A \cap \mathcal{C}$, V approximates the solution of the optimization problem. Furthermore, for all Γ for which $V(\Gamma) = v_2(\Gamma)$, we have the smooth-pasting condition $\nabla V = \nabla v_2$ ensured as well (see Ref. [26]), e.g., on the boundary $\partial(A \cap \mathcal{C})$.

Assuming that the process Q_t represents a wind resource on the site of a wind farm and Y_t the production as a function of Q_t, the class diagram as given in figure 1 represents a possible architecture for an object-oriented implementation with, e.g., `C++`. For integrating the stochastic differential equations, Runge-Kutta-type schemes as given in Ref. [24] or [33] with a convergence rate of $O(h)$ for step size $h \to 0$ are a suitable choice.

The performance requirements on any actual implementation are considerable. Given the periodic nature of the trend functions with cycle times as low as six hours in one case (see table A.2), as well as the high volatility in supply and demand, a resolution in the time dimension of 30 min per step is required for integrating the stochastic differential equations. This resolution already assumes an integration scheme of a convergence order $O(h)$, provided by, e.g., Runge-Kutta type

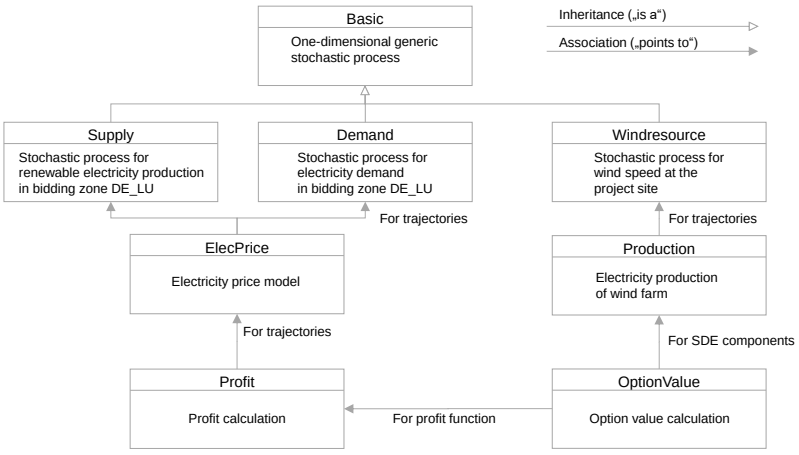

Figure 1: Proposed class diagram for implementation

schemes (see, e.g., [24], or [33]). We can demonstrate this requirement on resolution by comparing the electricity production of a hypothetical wind farm that is using empirical climatic data at first, and then comparing it against the production as a result of a wind speed forecast from eq. (6). This makes in particular the calculation of the profit function v_2 costly which requires to integrate supply, demand and wind speed over the life time of the investment, in high resolution and in a high number to calculate the average, for each point of time-to-invest. The subsequent Bellman-Howard approximation requires high computing power as well.

3 Example: an electrolyzer retrofit to an offshore wind farm

In this section, we give an example of the class of problems that our generalized approach is applicable to.

3.1 Electricity market model

The ENTSO-E transparency platform [10] provides downloads for total electricity consumption as well as for the total production data and separately for intermittent production from wind and solar, in 15 min values and for time zone CET/CEST. The data are normalized to hourly values and time zone GMT, to match climatic data used later on for the electricity production of the underlying wind farm. These time series, for the bidding zone DE_LU, can be analyzed with `R` (see [31], methods for time series analyses see Ref. [34]). Guided by spectral analysis, periodic time-dependent trend functions are found via regression, reported in appendix A.1, equations (A.1)-(A.5). The speed of reversion parameters are found with a numerical simulation, the mean and standard deviation of supply, demand and wind speed can be measured in the empirical data and, together with the speed of reversion parameters, lead to the volatility coefficients defined in eq. (3).

A current merit order curve can be found in [1], see figure 2a. A future merit order curve (figure 2b) can be estimated with the help of studies on the energy transition, such as in, e.g., [32].

For an overview of such studies, see Ref. [37] and in this meta study, [32] represents an average

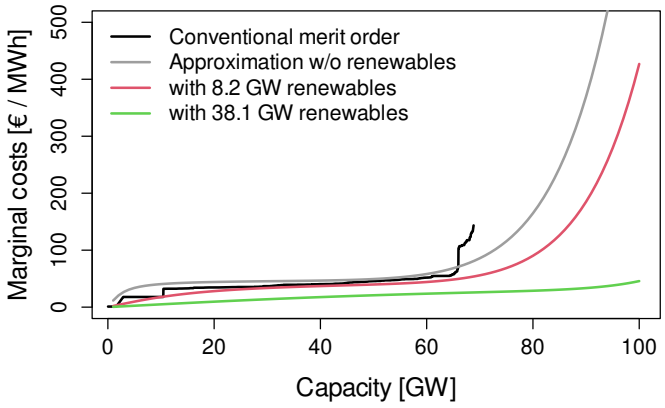

(a) Current conventional merit order curve [1], approximated, and with different scenarios for renewable power

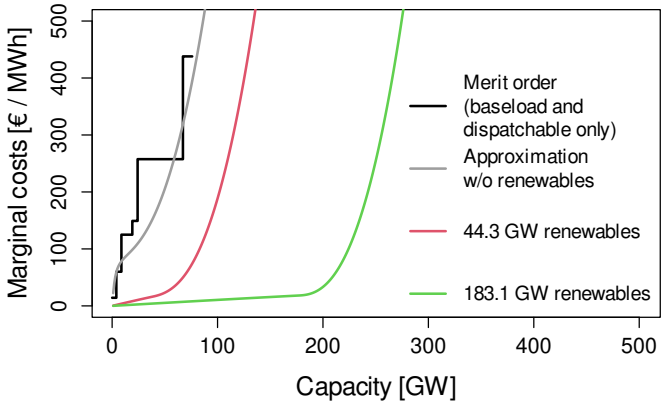

(b) Estimated future merit order curve [32], approximated, and with different scenarios for renewable power

Figure 2: Merit order curves

path to decarbonization. The data from [32] that we have used for estimating the future merit order, as well as most of the future demand, are listed in appendix A.2.

Based on this, parameter estimates for the supply function (eq. (4)) can be found with a numerical simulation. The parameters are reported in table 1, for the beginning and the end of a hypothetical time horizon that runs from today to the expected end state of the energy transition in Germany, i.e., to the year 2050, for which the policy target is carbon neutrality.

3.2 Parameters for the electrolyzer

In our example, we investigate the retrofit of an offshore wind farm with an electrolyzer. We assume that the offshore wind farm operates without subsidies, thus enabling it to sell its production on the day-ahead market for electricity. Let S^{H_2} be the hydrogen price, η be the electrolyzer efficiency, I the investment expenditure, C the variable costs of operation, and M the fixed costs of operation

Table 1: Parameters for the merit order list approximation

Parameter	Value at start	Value at end
α	0.088	0.400
c_1	2500	2500
c_2	30.5	57.0
c_3	0.00004	0.49150
c_4	1.55	2.91

(i.e. without capital costs). Then,

$$\pi_t = \begin{cases} Y_t \left(S^{H_2}\eta - S_t^E - C\right) & \text{for } S_t^E < S^{H_2}\eta - C \\ 0 & \text{otherwise} \end{cases}$$

is the gross profit rate. We regularize π with a convolution ([39], p.29) and use the same notation for the gross profit rate as defined above and for its regularization. The momentary value of the investment project is

$$v_t = \pi_t - M = \pi(Y_t, S^{H_2}, S_t^E(t, X_t)) - M(t)\,.$$

The project value for one trajectory of the process, starting at time t^* and going up to time t, is consequently represented as

$$\nu_{t,t^*}(S_t^E, Y_t) = \int_{t^*}^{t} v_s e^{-\rho s} ds - I\,.$$

The remaining parameters for the example are estimated as follows (t^* denotes the time to invest, P is the power of the electrolyzer):

- Investment expenditure $I = I(t^*, P)$; Ref. [32] estimates I at 1344 €/kW today and at 500 €/kW in the year 2050 (p.108)
- Efficiency $\eta = \eta(t^*) = 0.722$ as of today, see Ref. [37], p.5 or $\eta = 0.65$ in the year 2020 and $\eta = 0.7$ in the year 2050 (see Ref. [32], p.108)
- Other direct operating costs $C = C(t^*, P)$; Ref. [32] puts these at zero
- Other momentary operating and maintenance costs $M = M(t, t^*, P)$; estimated at 3% of the investment expenditures in [32]
- Hydrogen selling price S^{H_2}; [32] estimates a range of 0.118 - 0.126 €/kWh for hydrogen imports, which drives the price for domestic hydrogen production as well (p.100f).

3.3 Wind farm electricity production

For completing the example, we define the electricity production by selecting one of the subsidy-free offshore wind farms which is supposed to be commissioned soon in the German North Sea, Borkum Riffgrund 3, comprising 83 machines with 11 MW rating each (see company homepage [30] and planning approval notice [17]). For the electricity production of this wind farm, we estimate the power curves of the wind turbines at first piece-wise, following [40] where a simple cubic model

for the first part of the power curve is suggested and [21], which provides information on a suitable rated wind speed:

$$\tilde{P}(x) = \begin{cases} 0.0074x^3 & \text{for } 0 \le x < 11.1 \\ 0.47x + 4.76 & \text{for } 11.1 \le x < 13.3 \\ 11.0 & \text{for } 13.3 \le x < 24.9 \\ -27.5x + 693.0 & \text{for } 24.9 \le x < 25.1 \\ 0 & \text{for } x \ge 25.1 \end{cases}$$

(x in m/s, $\tilde{P}$ in MW), then and approximate it with a convolution $P(x) = (\tilde{P} * \Phi_\delta)(x)$, here with choosing the parameter value $\delta = 1.8$, to ensure a suitable shape for P (see figure 3). The wind

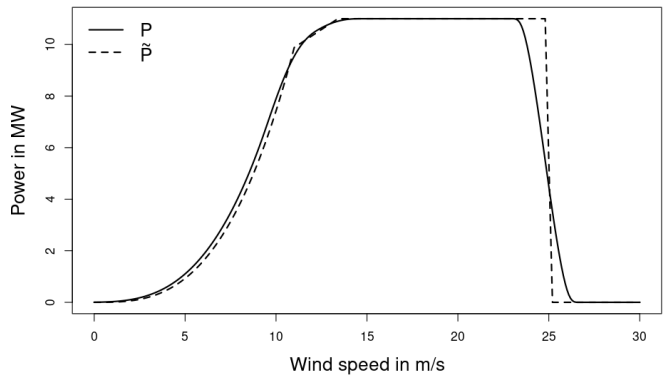

Figure 3: Generic power curve

farm is located between $54.0° - 54.1°$N and $6.0° - 6.3°$E (see Ref. [17]) and wind speed data can be accessed via the Copernicus Climate Change Service (C3S) Climate Data Store ([13]), in hourly resolution and for time zone GMT. The hub height used at this wind farm can be found in [17] and with this, a hub height correction in the wind speed is carried out (for measurements of the wind shear for an offshore wind farm see Ref. [35], for calculations see, e.g., [5], eq. (4)). As before, with `R`, the trend function $\kappa(t)$ for eq. (6) can easily be calculated. As mentioned before, it turns out that the wind farm electricity production is weekly cross-correlated to the renewable power generation, a fact that we consider while generating the random numbers for the numerical solution.

4 Numerical solution to the example

For the numerical calculations, we define the infinitesimal generator based on eq. (15) in difference form $L_\Delta = B_1\Delta_x + B_2\Delta_y + \Delta_t + 1/2(\Lambda_{11}\Delta_x^2 + \Lambda_{22}\Delta_y^2)$. With this, we define the difference operator for the option value Φ_Δ and the sequence of option values V_n by

$$\Phi_\Delta(V) = v_2 + [LV + (1-\rho)V - v_2]_+ \,, \quad V_{n+1} = \tilde{\Phi}(V_n), \quad \text{with start function } V_0 \,.$$

The operator Φ_Δ operates on the functions V for the total value and v_2 for the expected profit of the investment on the state space spanned by electricity price, production and time to invest $(S^E, Y) \times [0, \infty)$. For determining v_2, for each point in the state space, values are found via integrating the differential equations with the respective starting point, then averaging a number of trajectories and then evaluating the profit function. For convergence of the operator iteration, we use that Φ_Δ is Lipschitz with a constant $K > 0$ and ensure $K < 1$ by coordinate transformation. Further, in the bracket $[\cdot]_+$ above, one can see that for small LV, we must have $(1-\rho)V - v_2 > 0$ to find non-trivial solutions. Therefore, the starting point of each iteration is chosen above and close to v_2[7]. The usual stopping criterion for the iteration is the difference of adjacent elements of the approximation, i.e., $\|\|V_{n+1} - V_n\|\|_{L^2}$, sufficiently small. However, due to limitations in resolution that we must observe on standard hardware, error propagation may lead to oscillation (error handling and stability: e.g., [16]). Therefore, we add a second stopping criterion and stop in the first local minimum, whatever comes first. Going through the state space from $t = 0$ to

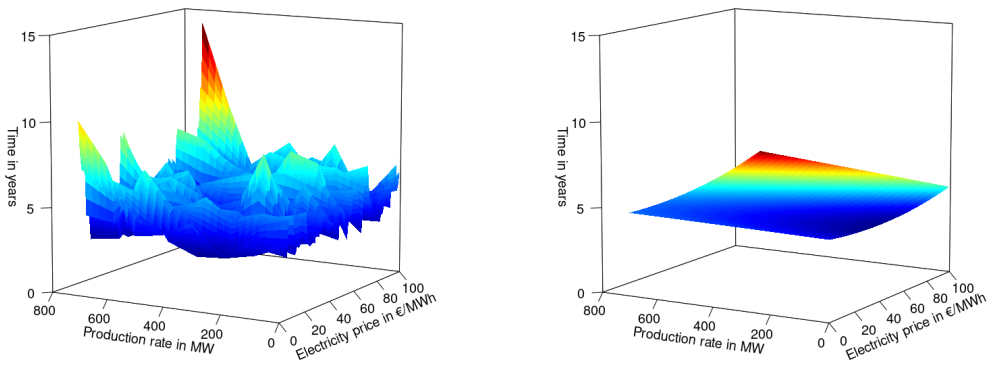

(a) Numerical result

(b) Regression

Figure 4: Surface that separates waiting from investing

$t = 35$ years, we find the surface at which $v_2 = V$, i.e., the surface that separates the continuation region (the region of waiting) from the stopping region (the region where the investment occurs at its beginning and the electrolyzer operates early on). As figure 4 shows, this surface is placed at very low points in time.

The numerical calculation for the stopping time tend to be imprecise because of the value matching $V(t^*) = v_2(t^*)$ and smooth pasting condition $V'(t^*) = v_2'(t^*)$ which are both fulfilled on the separation surface. For the error propagation from V and v_2 to t^*, we have, if t_A^* denotes an approximation for t^*:

$$\frac{V(t^*) - V(t_A^*) - v_2(t^*) + v_2(t_A^*)}{V'(t_A^*) - v_2'(t_A^*)} \approx t^* - t_A^* \,. \tag{16}$$

Both numerator and denominator on the left-hand side of eq. (16) are small. Given the challenge in error propagation that this is causing, we consider the remaining curvature that is visible in figure 4 as irrelevant. For practical considerations, figure 5 is more relevant as one can see how the intrinsic option value declines with waiting, and how it does so in relation to the profit function.

[7] Iterating downwards monotonically in the case of convergence; note that the case of a diverging iteration without any local minimum is possible, too. This would indicate an infinite option value and lead to the decision not to invest at all.

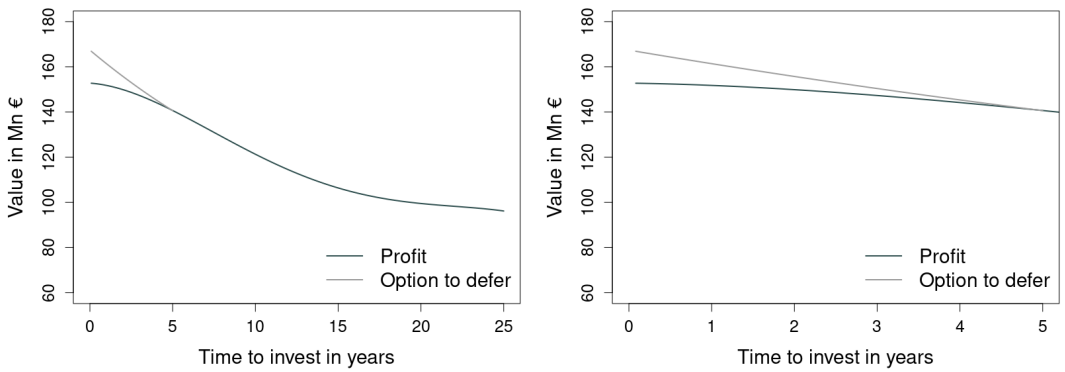

(a) Full time horizon

(b) Zoomed in

Figure 5: Profit as function of time to invest and option value to defer

5 Results, conclusions and outlook

The proposed generalized approach to optimal stopping makes use of the unique properties of the electricity market with its fully transparent time series for supply and demand and its quite good transparency on production costs. With its specific choice of stochastic differential equations, it captures the periodic behavior well, incorporates potential cross-correlations and thus, allows to calculate the option value to wait on a realistic basis, for a wide range of problems related to this market.

With our example, we can demonstrate the feasibility of the method. Firstly, we can provide a long-term forecast which is a pre-requisite for estimating effects in the ongoing energy transition with an end-to-end perspective. Secondly, we can show that once renewable power generation assets are exposed to fluctuating day-ahead markets, it becomes attractive for the private sector to invest in auxiliary technologies like electrolyzers without long waiting times – a step urgently required for a successful energy transition and thus important for policy making. The remaining rather small value of the option to defer may be overcome with, e.g., regulatory benefits for first movers or similar considerations.

Our approach leads to high numerical complexity. The periodic behavior shows cycle times as small as six hours per cycle and, therefore, it requires a high resolution in the time dimension. This, in combination with the long time horizons that are typical for assets in the energy market, in our example 35 years, requires a focus on performance in the numerical implementation. With the implementation we propose, the market forecast and the expected profit as a function of time to invest can be calculated with sufficient precision and acceptable calculation time. For the optimal stopping, with restricted resolution, this process is possible on standard hardware as well.

With that in mind, the main future research is to apply the method to further case studies with implications on energy policy, to e.g., other scenarios with a different mix of renewable power generation technologies, different storage technologies and subsequently with an alternative price development, or to other applications like investment in batteries etc. Ultimately, the goal is to support drafting new regulation that incentivize the private sector to take the next steps in the energy transition.

References

[1] Arnold et al. EWI Merit-Order Tool 2021. https://www.ewi.uni-koeln.de/de/publikationen/ewi-merit-order-tool-2021/, 2021. (Accessed on October 2, 2022).

[2] M. T. Barlow. A diffusion model for electricity prices. *Mathematical Finance*, 12(4):287–298, 2002.

[3] Veraart Barndorff-Nielsen, Benth. Modelling energy spot prices by lévy semistationary processes. *Preprint, CREATES Research Paper 2010-18*, 2010.

[4] Bundesamt für Wirtschaft und Ausfuhrkontrolle. Erdgasstatistik. https://www.bafa.de/DE/Energie/Rohstoffe/Erdgasstatistik/erdgas_node.html, 2022. (Accessed on October 10, 2022).

[5] Yiling Cai and François-Marie Bréon. Wind power potential and intermittency issues in the context of climate change. *Energy Conversion and Management*, 240:114276, 2021.

[6] Sören Christensen, Fabián Crocce, Ernesto Mordecki, and Paavo Salminen. On optimal stopping of multidimensional diffusions. *Stochastic Processes and their Applications*, 129(7):2561–2581, 2019.

[7] Sören Christensen and Albrecht Irle. The monotone case approach for the solution of certain multidimensional optimal stopping problems. *Stochastic Processes and their Applications*, 130(4):1972–1993, 2020.

[8] Savas Dayanik and Ioannis Karatzas. On the optimal stopping problem for one-dimensional diffusions. *Stochastic Processes and their Applications*, 107(2):173–212, 2003.

[9] A.K. Dixit and R.S. Pindyck. *Investment Under Uncertainty*. Princeton University Press, 1994.

[10] ENTSO-E. Actual generation by production type, for Bidding Zone Germany BZN DE-LU. https://transparency.entsoe.eu/generation/r2/actualGenerationPerProductionType/show, 2022. (Accessed on October 2, 2022).

[11] ENTSO-E. Installed Capacity per Production Type, for Bidding Zone Germany BZN DE-LU. https://transparency.entsoe.eu/generation/r2/installedGenerationCapacityAggregation/show, 2023. (Accessed on April 9, 2023).

[12] ENTSO-E Transparency Platform. EIC Approved Codes. https://www.entsoe.eu/data/energy-identification-codes-eic/eic-approved-codes/, 2022. (Accessed on October 11, 2022).

[13] Hersbach et al. ERA5 hourly data on single levels from 1959 to present. https://cds.climate.copernicus.eu/cdsapp#!/dataset/reanalysis-era5-single-levels?tab=form, 2018. (Accessed on August 12, 2022).

[14] Gebeyehu M. Fetene, Sigal Kaplan, Stefan L. Mabit, Anders F. Jensen, and Carlo G. Prato. Harnessing big data for estimating the energy consumption and driving range of electric vehicles. *Transportation Research Part D: Transport and Environment*, 54:1–11, 2017.

[15] Stefan Franzen and Reinhard Madlener. Optimal expansion of a hydrogen storage system for wind power (H2-WESS): A real options analysis. *Energy Procedia*, 105:3816–3823, 2017. 8th International Conference on Applied Energy, ICAE2016, 8-11 October 2016, Beijing, China.

[16] R.W. Freund and R.W. Hoppe. *Stoer/Bulirsch: Numerische Mathematik 1*. Springer-Lehrbuch. Springer Berlin Heidelberg, 2007.

[17] Bundesamt für Seeschifffahrt und Hydrographie. Planfeststellungsbeschluss. https://www.bsh.de/DE/THEMEN/Offshore/_Anlagen/Downloads/Genehmigungsbescheid/Windparks/PFB_Borkum_Riffgrund_3.pdf?__blob=publicationFile, 2021. (Accessed on August 12, 2022).

[18] Hélyette German and Andrea Roncoroni. Understanding the fine structure of electricity prices. *Journal of Business*, 79(3):1225–1261, 2006.

[19] Marcus Hildmann, Andreas Ulbig, and Göran Andersson. Revisiting the merit-order effect of renewable energy sources. In *2015 IEEE Power & Energy Society General Meeting*, 2015.

[20] John Hull and Alan White. One-factor interest-rate models and the valuation of interest-rate derivative securities. *The Journal of Financial and Quantitative Analysis*, 28(2):235–254, 1993.

[21] J Jonkman, S Butterfield, W Musial, and G Scott. Definition of a 5-MW reference wind turbine for offshore system development. *NREL Technical Report*, TP-500(38060), 2 2009.

[22] I. Karatzas and S.E. Shreve. *Brownian Motion and Stochastic Calculus*. Graduate Texts in Mathematics (Book 113). Springer New York, 1991.

[23] Dogan Keles and Joris Dehler-Holland. Evaluation of photovoltaic storage systems on energy markets under uncertainty using stochastic dynamic programming. *Energy Economics*, 106:105800, 2022.

[24] P. E. Kloeden and R. A. Pearson. The numerical solution of stochastic differential equations. *The Journal of the Australian Mathematical Society. Series B. Applied Mathematics*, 20(1):8–12, 1977.

[25] Kraftfahrtbundesamt. Fahrzeugbestand am 01. Januar 2021. https://www.kba.de/DE/Presse/Pressemitteilungen/Fahrzeugbestand/2021pm08_fz_bestand_pm_komplett.html;jsessionid=6F07E5BAACF46FD56562898172DC90EA.live21324, 2021. (Accessed on October 22, 2022).

[26] N.V. Krylov. *Controlled Diffusion Processes*. Stochastic Modelling and Applied Probability. Springer Berlin Heidelberg, 2008.

[27] Nicolas Langrené, Geoffrey Lee, and Zili Zhu. Switching to Non-Affine Stochastic Volatility: A Closed-Form Expansion for the Inverse Gamma Model. *Econometrics: Econometric & Statistical Methods - Special Topics eJournal*, 2015.

[28] Daniel B. Nelson. ARCH models as diffusion approximations. *Journal of Econometrics*, 45(1):7–38, 1990.

[29] Ofgem Office of Gas and Electricity Markets UK. Bidding Zones Literature Review. https://www.ofgem.gov.uk/sites/default/files/docs/2014/10/fta_bidding_zone_configuration_literature_review_1.pdf, 2014. (Accessed on October 11, 2022).

[30] Ørsted. Borkum Riffgrund 3. https://orsted.de/gruene-energie/offshore-windenergie/unsere-offshore-windparks-nordsee/offshore-windpark-borkum-riffgrund-3. (Accessed on August 10, 2022).

[31] R Core Team. R: A language and environment for statistical computing. https://www.R-project.org/, 2021.

[32] Martin Robinius, Peter Markewitz, Peter Lopion, Felix Kullmann, Chloi Syranidou, Simonas Cerniauskas, Markus Reuß, David Ryberg, Leander Kotzur, Dilara Caglayan, Lara Welder, Jochen Linssen, Thomas Grube, Heidi Heinrichs, Peter Stenzel, and Detlef Stolten. *WEGE FÜR DIE ENERGIEWENDE Kosteneffiziente und klimagerechte Transformationsstrategien für das deutsche Energiesystem bis zum Jahr 2050*. Forschungszentrum Jülich, July 2020.

[33] Timothy Sauer. Computational solution of stochastic differential equations. *Wiley Interdisciplinary Reviews: Computational Statistics*, 5, 2013.

[34] R.H. Shumway and D.S. Stoffer. *Time Series Analysis and Its Applications: With R Examples*. Springer Texts in Statistics. Springer International Publishing, 2017.

[35] Anders Sommer. Wind Resources at Horns Rev. `https://www.yumpu.com/en/document/view/4469663/wind-resources-at-horns-rev`, 2002. (Accessed on October 9, 2022).

[36] Rafał Weron. Electricity price forecasting: A review of the state-of-the-art with a look into the future. *International Journal of Forecasting*, 30(4):1030–1081, 2014.

[37] Frauke Wiese, Johannes Thema, and Luisa Cordroch. Strategies for climate neutrality. Lessons from a meta-analysis of German energy scenarios. *Renewable and Sustainable Energy Transition*, 2:100015, 2022.

[38] Klaas Würzburg, Xavier Labandeira, and Pedro Linares. Renewable generation and electricity prices: Taking stock and new evidence for Germany and Austria. *Energy Economics*, 40:S159–S171, 2013. Supplement Issue: Fifth Atlantic Workshop in Energy and Environmental Economics.

[39] K. Yosida. *Functional Analysis*. Classics in Mathematics. Springer Berlin Heidelberg, 2012.

[40] D.P. Zafirakis, A.G. Paliatsos, and J.K. Kaldellis. 2.06 - energy yield of contemporary wind turbines. In Ali Sayigh, editor, *Comprehensive Renewable Energy*, pages 113–168. Elsevier, Oxford, 2012.

A Appendix

A.1 Electricity market model

A.1.1 Supply trend functions today

Based on a spectral analysis of the electricity production data in bidding zone DE_LU, year 2019, we find the following regressions in the data from [10]. For electricity production from wind power:

$$\mu_1^{(1)}(t) = 14185.8 + 5721.8\cos\left(\frac{2\pi t}{8760}\right) + 1313.8\sin\left(\frac{2\pi t}{8760}\right). \tag{A.1}$$

For production from solar power, the complete regression is easiest constructed as the product of daily and annual cycle: $\mu_2^{(1)}(t) = \mu_{2,A}^{(1)} \cdot \mu_{2,D}^{(1)}$, with the annual trend

$$\mu_{2,A}^{(1)}(t) = 1 + 0.9\cos\left(\frac{2\pi t}{8760} + 3.3\right) \tag{A.2}$$

formulated as a factor to the daily trend, where the daily trend is given as

$$\mu_{2,D}^{(1)}(t) = 4784.9 + \sum_{i=1}^{4} C_i\cos\left(\frac{2\pi\omega_i t}{8760}\right) + D_i\sin\left(\frac{2\pi\omega_i t}{8760}\right). \tag{A.3}$$

The frequencies and coefficients are reported in table A.1. With the product formulas for trigonometric functions, this trend function can be transformed into a linear combination of sin and cos, as required in section 2.1.

Table A.1: Parametrization of the daily pattern in solar production, year 2019

i	Frequency ω_i in cycles per year	Time per cycle (h)	Coefficients	
			C_i	D_i
1	365	24	-7397.2	512.7
2	730	12	3123.6	-492.7
3	1095	8	-322.8	150.9
4	1460	6	-271.8	39.4

A.1.2 Demand trend functions today

The load profile for the total electricity demand can be found in two steps. First, an annual cycle is determined and taken out of the data.

$$\mu_1^{(2)}(t) = 57198.7 + 3741.2\cos\left(\frac{2\pi t}{8760}\right) + 675.4\sin\left(\frac{2\pi t}{8760}\right) \quad \text{(in MW)}. \tag{A.4}$$

Second, the more complex weekly and daily pattern is found in the data for year 2019, restricted to February 2019 (four weeks), with identifying the required frequencies first with spectral analysis. The trend function is

$$\mu_2^{(2)}(t) = 1550.3 + \sum_{i=1}^{11} A_i\cos\left(\frac{2\pi\omega_i(t-72)}{672}\right) + B_i\sin\left(\frac{2\pi\omega_i(t-72)}{672}\right), \tag{A.5}$$

the frequencies and the coefficients are reported in table A.2. With this construction, the holiday

Table A.2: Parametrization of weekly and daily periodic fit, February 2019

i	Frequency ω_i, in cycles per four weeks	Time per cycle	Coefficients	
			A_i	B_i
1	4	1 week	2188.1	-5916.3
2	8	84 h	2834.2	2644.5
3	12	56 h	-1309.5	-
4	16	42 h	1078.9	-
5	20	33 h 36 min	-1295.8	1067.2
6	24	28 h	-564.8	-1487.9
7	28	24 h	-7379.7	-3653.9
8	32	21 h	-	989.0
9	56	12 h	-1603.0	-3932.9
10	60	11 h 12 min	-427.0	592.2
11	112	6 h	685.1	651.9

period at the beginning and the end of each year, which is clearly visible in the empirical data, is deliberately ignored, as this does not add any relevant information to the model but complicates the regression considerably.

A.2 Future system state

Ref. [37] gives an overview of the studies on energy transition in Germany with the common goal of mitigating at least 95% of greenhouse gases until year 2050. The study [32] is among those and represents an average path among all studies mentioned. The main statements from [32] for the future system state in the year 2050, relevant to our example, are listed here.

With its estimated electricity production, reported in table A.3, the future consumption can be estimated and with this, the future trend functions are established. With the help of estimated

Table A.3: Electricity production by type

Production type	Year 2019 [TWh]	Year 2050 [TWh]
Wind	124.6	671.9
Solar	42.0	192.7
Biomass	40.6	47.7
Run-of-river hydro	14.6	14.6
Other renewable	1.5	74.5
Other	314.1	-
Balance	-	6.6
Total	537.3	1008.0

Sources:
Year 2019: [10]
Year 2050: [32], pp.24, 27, 30, 33; [10]
Run-of river hydro assumed to remain constant

future capacity (table A.4) and estimated future operating costs (table A.5), the future merit order curve is constructed. The demand is based on the capacity and electricity volume quoted

Table A.4: Generation and storage capacity by type in year 2050

Capacity type	Capacity [GW]	[%]
Onshore wind	221.0	44%
PV - greenfield	104.0	21%
PV - rooftop	63.0	13%
Fuel cells, gas turbines	43.0	
Offshore wind	33.0	
Pumped storage hydro	10.4	
Biomass	8.8	
Compressed air energy storage	5.0	
Batteries	4.8	
Run-of river hydro	4.0	
Total	497.0	

Source: [32], pp. 4, 25-28, 31-33, [11], [25]
Run-of river hydro assumed to remain constant

from [32], but the future profile requires additional considerations. Among other sectors, also the building sector is expected to be electrified and, therefore, a much stronger seasonal profile in electricity consumption with a higher consumption in winter can be expected. Therefore, the

Table A.5: Operating costs in year 2050

Technology	Operating costs (€/kWh)
PV - greenfield	0.010
Onshore wind	0.011
Run-of-river hydro	0.014
PV - rooftop	0.017
Offshore wind	0.025
Batteries (market value)	0.060
Pumped storage hydro	0.125
Compressed air energy storage	0.149
Fuel cells and Gas turbines	0.258
Biomass	0.438
Batteries (full costs)	4.130

Source: [32], pp. 28, 32, 103ff; [10], [11]; own calculations

amount of electricity required for heating is distributed in line with the profile of gas consumption (Ref. [4]) today.

The same consideration is applied to the transportation sector. Here, e.g., Ref. [14] provides information on the temperature dependency of battery-electric vehicles.